# A Pressure Equation for Weakly Compressible SPH

Kalale Chola[a,b,*], Tsumoru Shintake[c]

[a] *Quantum Wave Microscopy Unit, OIST Graduate University, 1919-1 Tancha, Onna-son, Okinawa 904-0495*
[b] *Fluid Mechanics Unit, OIST Graduate University, 1919-1 Tancha, Onna-son, Okinawa 904-0495*
[c] *Quantum Wave Microscopy Unit, OIST Graduate University, 1919-1 Tancha, Onna-son, Okinawa 904-0495*

**Abstract**

This paper presents a formulation of a general form of an equation for pressure using thermodynamic principles. The motivation for this is in large part due to the need for a pressure equation for smoothed particle hydrodynamics, SPH, that takes into account the role of entropy. This is necessary because the use of physical and artificial viscosity leads to an increase in entropy. While such an increase in entropy in liquids may be negligibly small, standard SPH formulations treat a liquid as a weakly compressible gas. Consequently, for fluid-fluid and fluid-structure impact flows, the resulting increase in entropy is not negligible anymore. The proposed pressure equation contains diffusion terms whose main role is to smooth out unphysically large numerical oscillations in the pressure field related to the shock during an impact event. One consequence of adopting this numerical scheme, however, is that there are new (free) parameters that must be set. Nevertheless, effort has been made to obtain their plausible estimators from physical principles. The

*Corresponding author
*Email address:* Kalale-Chola1@oist.jp (Kalale Chola)

proposed model is applicable outside the domain of SPH.

*Keywords:* pressure equation, generalized EDAC, incompressibility modulus, SPH, thermodynamics

## 1. Introductions

In weakly compressible SPH (WCSPH), artificial incompressibility is introduced via a simple equation of state on the basis that the flow is isentropic i.e. zero thermal diffusivity. This was originally proposed by Monaghan [1].

$$P = \mathrm{B}\left[\left(\frac{\rho}{\rho_0}\right)^{\gamma} - 1\right] \tag{1}$$

where $P$ is the pressure, $\rho$ is the density and $\rho_0$ is the reference density when $P = 0$. The stiffness parameter B is given by defining a reference speed of sound $c_0^2 := (\partial P/\partial\rho)|_{\rho=\rho_0} = B\gamma/\rho_0$ and the parameter $\gamma$ is typically chosen to be $\gamma = 7$ for water and $\gamma = 1$ for air. With this stiff equation of state, small errors in the density lead to very large spurious noise in the pressure field which in turn pollutes the computed velocity field. In particular, within the realm of weakly compressible fluids, one can consider density fluctuations $\Delta\rho := \rho - \rho_0$ with an additional assumption that these fluctuations are small i.e. $|\Delta\rho/\rho_0| \ll 1$. Then using the binomial expansion of $(1 + \Delta\rho/\rho_0)^{\gamma}$ for small $\Delta\rho$ in equation (1), a less stiff equation of state proposed by Müller et al. [2] is obtained:

$$P = c_0^2(\rho - \rho_0) \tag{2}$$

Note the similarity of (2) to the ideal gas law, with the exception of the background pressure $-\rho_0 c_0^2$ which is essential for numerical stability of the

simulation [2]. Furthermore, due to the isentropic flow assumption, both equations of state (1) and (2) may not be adequate in capturing the pressure correctly for viscous flows within the weak compressibility SPH framework. Due to the use both physical and artificial viscosity, entropy increases. While the role of entropy in liquids can be neglected, in WCSPH, a liquid is treated as a weakly compressible gas. Therefore, on this basis, the role of entropy in computing the pressure must be taken into account particularly for fluid flows involving impact.

The WCSPH scheme has been successfully applied to the simulation of astrophysical problems, multiphase flows, free surface flows, fluid-structure interaction, elastic fracture, thermal and matter diffusion, physiological problems and many others [3]. It remains a popular approach as it makes it possible to write the system equations as an hyperbolic system that can be integrated in a simple manner. However, the use of a stiff equation of state for pressure in WCSPH schemes sometimes leads to large, spurious numerical high-frequency oscillations in the predicted pressure field. To mitigate this problem, several correction algorithms have been proposed in the literature. Colagrossi and Landrini [4] suggested to periodically re-initialize the density field every 20-40 time steps with a moving least square (MLS) integral interpolation. While this method is effective at reducing the unphysical pressure oscillations, it does not guarantee long term stability of the pressure field due to the loss of volume conservation; mismatch between density and volume represented by fluid particles accumulates as the density is calculated by a time-advancing manner. The third and particularly attractive approach is the introduction of diffusion terms into the continuity equation

as proposed by Antuono et al. [5]. The introduction of these artificial terms is perhaps less rigorous when compared with the EDAC approach which is premised on a physically sound basis [6]. The EDAC scheme has recently attracted some attention in the fluid dynamics community; Ramachandran and Puri [7], Toutant [8], Kajzer and Pozorski [9], Dupuy et al. [10]. Unlike the Poisson equation, the EDAC method is fully explicit requiring no sub-iterations. This implies that the EDAC method has a lower computational cost for incomperessible flow simulations. The aforementioned studies have further demonstrated that the EDAC method has low memory requirements and is easily paralellizable as the system of equations are explicit in time.

One common way of modeling the incompressible Navier-Stokes equations (INS) is to assume that the fluid compressibility is zero. In such an ideal fluid, pressure disturbances are transmitted instantaneously. As noted by Clausen [6], the instantaneous propagation of pressure fluctuations across the entire fluid domain results in an elliptic-type system that requires non-local communication. The Poisson pressure equation (PPE) in incompressible SPH presents a challenge in speeding up SPH computations as it involves solving a large, sparse matrix, that must be solved on an entire computational domain; small perturbations near boundaries or free surfaces can instantaneously propagate across the entire domain and may lead to large numerical oscillations and instabilities in the numerical solution [11]. This means that the INS is sensitive to numerical oscillations and it is consequently easier to induce numerical instabilities.

The structure of the paper is organized as follows: In the subsequent section, a detailed formulation of the pressure equation is presented with

careful consideration of relevant thermodynamic properties. Then the theoretical considerations of the parameters fundamental to this work are discussed in some detail. Finally, in the section on model validation, a number of benchmark problems are computed using the proposed model and the EDAC scheme, and the computational results are validated against experimental data or analytical solutions if available.

## 2. Pressure equation

### *2.1. Background*

The analysis begins with the fundamental equations of fluid mechanics, namely the compressible Navier-Stokes equations:

$$\frac{d\rho}{dt} = -\rho \boldsymbol{\nabla} \cdot \mathbf{u} \tag{3a}$$

$$\rho \frac{d\mathbf{u}}{dt} = -\boldsymbol{\nabla} P + \rho\nu\nabla^2\mathbf{u} + \rho\boldsymbol{g} \tag{3b}$$

$$\rho \frac{du}{dt} = -P\boldsymbol{\nabla} \cdot \mathbf{u} + \boldsymbol{\nabla} \cdot (k\boldsymbol{\nabla} T) + \Phi \tag{3c}$$

In the above equations the symbols have the following meaning: fluid density $\rho$, fluid pressure $P$, fluid velocity $\mathbf{u}$, kinematic viscosity $\nu$, acceleration due to gravity $\boldsymbol{g}$, temperature $T$, specific internal energy $u$, thermal conductivity $k$, and dissipation function $\Phi = \rho\nu(\boldsymbol{\nabla}\mathbf{u} + \boldsymbol{\nabla}\mathbf{u}^{\mathrm{T}}) : \boldsymbol{\nabla} u$.

When incompressibility $\boldsymbol{\nabla} \cdot \boldsymbol{u} = 0$ is assumed, the system of equations (3) can be closed by taking the divergence of the conservative form of the momentum equation (3b) to obtain an equation for pressure, namely the pressure Poisson equation, PPE, given by $\nabla^2 P = -\boldsymbol{\nabla}\boldsymbol{u} : \boldsymbol{\nabla}\boldsymbol{u}^{\mathrm{T}}$. This is the equation (or its variants in SPH) that is solved in incompressible SPH

to obtain the pressure field. Instead of solving an elliptic system, the incompressibility requirement can be relaxed. WCSPH accomplishes this by using either (1) or (2) above and evolving the density according to equation (3a). Clausen [6] proposed the entropically damped artificial compressibility (EDAC) model:

$$\frac{d\mathbf{u}}{dt} = -\frac{1}{\rho_0}\boldsymbol{\nabla} P + \nu\nabla^2\mathbf{u} + \boldsymbol{g} \tag{4a}$$

$$\frac{dP}{dt} = -\rho_0 c_0^2 \boldsymbol{\nabla}\cdot\mathbf{u} + \nu\nabla^2 P \tag{4b}$$

where thermodynamic parameters subscripted with a zero are reference quantities when $P = 0$; speed of sound $c_0$, and reference density $\rho_0$.

Note that while the pressure equation (4b) is for quasi-incompressible flows, a similar equation was proposed by Zang et al. [12] in the context of compressible flow dynamics. One key assumption made by Clausen [6] is that there are no thermodynamic fluctuations in the density $d\rho = 0$, i.e. fluid density is constant. This enabled him to express temperature gradients in terms of pressure gradients via a simple linear relation. In our analysis this assumption shall be relaxed. This is to be consistent with the assumption of weak compressibility where $d\rho$ is small but not necessarily zero.

Although in SPH calculations the volume is not computed directly, we can use the volume estimator $V = m/\rho$ where $m$ is the mass. Then the change in volume can be estimated as $dV = -md\rho/\rho^2$. Using this volume estimator, quantities can either be expressed in terms of per unit mass or per unit volume. These transformations shall be used in the next section where we have adopted the per unit volume convention since it is typical to use $V$ as a state function in thermodynamics rather than $\rho$.

*2.2. Formulation: thermodynamics of the fluid*

First, observe that the motion of a compressible fluid is directly affected by its thermodynamic state, itself a consequence of the motion. This has a profound consequence that the thermodynamic principles underpinning the first and second laws of thermodynamics are fundamental to the theory of compressible flows. The fact that any change in the state of the fluid is independent of the actual physical process by which the change was achieved makes thermodynamics powerful. This makes it possible to combine the first and second laws of thermodynamics to obtain the famous Gibbs equation which is stated exclusively in terms of exact differentials.

To begin our exposition, we briefly consider the notion of work and heat next. First we define a state space $\sum$ as an open, simply connected subset $\sum \subset (0,\infty)\times(0,\infty)$. The elements of $\sum$ are called states; of which the most fundamental are pressure P, internal energy U, and volume V. We define a path $\Gamma$ for our model to be an oriented, continuous, piecewise $C^1$ curve in the state space. This is then parameterized by writing:

$$\Gamma := \{(U(\mathbf{r}(t),t), V(\mathbf{r}(t),t)) \mid \ t \in \mathscr{I} = [t_1,t_2]\} \tag{5}$$

The first law of thermodynamics for our thermodynamic system i.e. a fluid parcel is given by

$$\delta Q = dU + \delta W \tag{6}$$

where $\delta Q$ is the heat added to the system (per unit volume) with the net heat gained $\mathbb{Q}(\Gamma) := \int_\Gamma \delta Q$. Similarly, $\delta W$, is the work done by compression and expansion of the fluid parcel with $\mathbb{W}(\Gamma) := \int_\Gamma \delta W \equiv \int_V P dV$. Note that the

notation $\delta$ is used here for the differentials to emphasize that both $\delta Q$ and $\delta W$ are path dependent. This obviously means that both $\mathbb{Q}$ and $\mathbb{W}$ do not qualify as state functions. The internal energy, on the other hand, is a state function and is thus expressed as an exact differential using the notation $d$. Any change in the internal energy of the system is equal to the difference between the final and initial values irrespective of the path followed by the system between the two states 1 and 2 since $\int_1^2 dU = U_2 - U_1$. The system in this case would be an infinitesimal fluid element. For the fluid, the first law of thermodynamics (6) is only useful if we can determine a functional relationship between the internal energy, volume and pressure $P = P(U, V)$. Assuming that an equation of state, or alternatively an evolution equation for pressure, can be found, the first law of thermodynamics becomes:

$$\delta Q = dU + P(U, V)dV \tag{7}$$

According to Pfaff's theorem (7) has an integration factor $1/T(U, V)$ (postulated in the zeroth law of thermodynamics) that transforms it into an exact differential form.

$$\frac{\delta Q}{T(U, V)} = \frac{1}{T(U, V)}dU + \frac{P(U, V)}{T(U, V)}dV \equiv dS(U, V) \tag{8}$$

which implies the existence of two new state functions which are the temperature $T(U, V)$ and an associated integral called the entropy $S(U, V)$. The final result is Gibbs equation.

$$dU = TdS - PdV \tag{9}$$

Using the volume estimator $V = m/\rho$ where $m$ is the mass, then the change in volume can be estimated as $dV = -md\rho/\rho^2$. In terms of quantities per

unit mass variables instead of per unit volume (i.e. $du$ instead of $dU$ with $u = U/m$), Gibbs equation can be expressed as $du = Tds - Pd\rho/\rho^2$. However, since thermodynamic capacities (to be discussed shortly) are typically expressed in terms of per unit volume quantities, we shall use the per unit volume quantities for the rest of the discussion. It is nevertheless straightforward to switch between the two conventions. Furthermore, thermodynamic properties such as $S$, $U$, $V$ and $m$ are additive and are called extensive properties; they depend on the mass of the thermodynamic system. By contrast, $P$, $T$ and $\rho$ are nonadditive and are called intensive properties; they do not depend on the size of the thermodynamic system. The ratio between any two extensive properties is an intensive property so that specific internal energy $u = U/m$, specific entropy $s = S/m$ and density $\rho = m/V$ are all intensive properties. Extensive properties are symbolized by uppercase letters whereas intensive properties are symbolized by lowercase letters. Exceptions are temperature $T$ and mass $m$.

Our goal is to determine $dP(U, V)$. Starting with the differential form for U:

$$dU = \left(\frac{\partial U}{\partial S}\right)_V dS + \left(\frac{\partial U}{\partial V}\right)_S dV \tag{10}$$

From (9) and (10) we then have

$$T = \left(\frac{\partial U}{\partial S}\right)_V, \qquad P = -\left(\frac{\partial U}{\partial V}\right)_S \tag{11}$$

However, $dU$ is an exact differential and by Clairaut's theorem second derivatives of partials are the same irrespective of the order of differentiation. We

then obtain an important relation for the system parameters.

$$\left(\frac{\partial T}{\partial V}\right)_S = -\left(\frac{\partial P}{\partial S}\right)_V \tag{12}$$

which happens to be one of the classical Maxwell's relations for thermodynamics. Since $U = U(S, V)$, we then infer that $T = T(S, V)$ and $P = P(S, V)$. Using these important relations, we proceed to compute the differential form for the pressure.

$$dP = \left(\frac{\partial P}{\partial S}\right)_V dS + \left(\frac{\partial P}{\partial V}\right)_S dV \tag{13}$$

In order to obtain the material derivative of the pressure, we first use Gibbs equation (9) to eliminate $dS$ from equation (13) yielding;

$$dP = \frac{1}{T}\left(\frac{\partial P}{\partial S}\right)_V dU + \left\{\left(\frac{\partial P}{\partial V}\right)_S + \frac{P}{T}\left(\frac{\partial P}{\partial S}\right)_V\right\} dV \tag{14}$$

The goal is to find equivalent partial derivatives containing $P$, $T$ and $V$ that are physically measurable and thus provides a means for determining the change of pressure with entropy, which is not measurable. To this end, we now introduce useful thermodynamic capacities given by the following relations.

$$K_S := -V\left(\frac{\partial P}{\partial V}\right)_S, \quad K_T := -V\left(\frac{\partial P}{\partial V}\right)_T, \quad \beta := \frac{1}{V}\left(\frac{\partial V}{\partial T}\right)_P \tag{15}$$

where $K_S$ is the adiabatic incompressibility modulus, $K_T$ is the isothermal incompressibility modulus and $\beta$ is the volumetric thermal expansivity. Since $K_S, K_T < 0$ contradicts mechanical stability, all materials have $K_S, K_T > 0$. There is no general principle that could limit $\beta$. However, fluids and most materials expand upon heating so that $\beta > 0$. To determine the coefficient

of $dU$ in (14), we first determine the isochoric change in pressure with temperature. Using the Jacobian transform:

$$\begin{aligned}
\frac{\partial(S,T)}{\partial(P,T)} &= \frac{\partial(S,T)}{\partial(V,T)} \cdot \frac{\partial(V,T)}{\partial(P,T)} \\
\implies \left(\frac{\partial S}{\partial P}\right)_T &= \left(\frac{\partial S}{\partial V}\right)_T \cdot \left(\frac{\partial V}{\partial P}\right)_T \\
\implies -\left(\frac{\partial V}{\partial T}\right)_P &= +\left(\frac{\partial P}{\partial T}\right)_V \cdot \left(\frac{\partial V}{\partial P}\right)_T \\
\therefore \left(\frac{\partial P}{\partial T}\right)_V &= -V\left(\frac{\partial P}{\partial V}\right)_T \cdot \frac{1}{V}\left(\frac{\partial V}{\partial T}\right)_P = K_T\beta
\end{aligned} \tag{16}$$

where use has been made of of Maxwell's relations (see Appendix A) in the third equality. Finally, using the above result, we then have

$$\begin{aligned}
\frac{\partial(P,V)}{\partial(S,V)} &= \frac{\partial(P,V)}{\partial(T,V)} \cdot \frac{\partial(T,V)}{\partial(S,V)} \\
\left(\frac{\partial P}{\partial S}\right)_V &= \frac{\beta T K_T}{C_V}
\end{aligned} \tag{17}$$

where $C_V := T(\partial S/\partial T)_V$ is the heat capacity at constant volume. With the relation given by equation (17), the pressure differential form (14) can then be expressed in terms of thermodynamic capacities:

$$dP = \frac{\beta K_T}{C_V} dU + \left(\frac{\beta K_T}{C_V} P - \frac{K_S}{V}\right) dV \tag{18}$$

Furthermore, using the continuity equation (3a) with $dV = -m d\rho/\rho^2$ and the energy equation (3c) with $u := U/m$, equation (18) takes the form

$$\frac{dP}{dt} = -K_S \boldsymbol{\nabla} \cdot \mathbf{u} + \frac{\beta V K_S}{C_p} \Phi + \frac{\beta V K_S}{C_V} \boldsymbol{\nabla} \cdot (k \boldsymbol{\nabla} T) \tag{19}$$

using the thermodynamic relation $\gamma = C_p/C_V = K_S/K_T$.

### 2.3. Temperature gradient estimate

The next step is to eliminate the temperature from the above equation. To achieve this, we introduce pressure as a thermodynamic state function of temperature and volume i.e. $P \equiv P(T, V)$. The associated differential form becomes

$$\begin{aligned} dP &= \left(\frac{\partial P}{\partial T}\right)_V dT + \left(\frac{\partial P}{\partial V}\right)_T dV \\ &= \beta K_T dT - \frac{K_T}{V} dV \end{aligned} \tag{20}$$

In the standard EDAC scheme, Clausen [6] proceeds by imposing a constraint that there are no thermodynamic fluctuations in the density i.e. $d\rho = 0$ or equivalently $dV = 0$ to obtain a thermodynamic relationship between pressure gradients and temperature gradients. In principle, imposing a constraint such as $d\rho = 0$ would be computationally demanding in the sense that one has to continually check that at each time integration step, this condition is met (or is at least below a prescribed threshold), akin to INS solvers where the condition $\boldsymbol{\nabla} \cdot u = 0$ has to be checked.

Therefore, with this background, we proceed without the additional constraint $d\rho = 0$ or equivalently $dV = 0$. Then from equation (20), we have

$$\boldsymbol{\nabla} T = \frac{\boldsymbol{\nabla} V}{\beta V} + \frac{\gamma}{\beta K_S} \boldsymbol{\nabla} P, \quad \text{alternatively} \quad \boldsymbol{\nabla} T = -\frac{\boldsymbol{\nabla} \rho}{\beta \rho} + \frac{\gamma}{\beta K_S} \boldsymbol{\nabla} P \tag{21}$$

Simplifying (19) and (21) gives:

$$\frac{1}{K_S} \frac{dP}{dt} = -\boldsymbol{\nabla} \cdot \mathbf{u} + \frac{\beta}{\rho c_p} \Phi + \frac{\beta}{\rho c_p} \boldsymbol{\nabla} \cdot \left(\frac{\gamma k}{\beta K_S} \boldsymbol{\nabla} P\right) - \frac{\beta}{\rho c_p} \boldsymbol{\nabla} \cdot \left(\frac{k}{\beta \rho} \boldsymbol{\nabla} \rho\right) \tag{22}$$

where the specific heat capacity is defined as the heat capacity per unit mass i.e. $c_p := C_P/m$. Note that $\gamma > 1$ for all substances so that $K_S > K_T > 0$

and $C_P > C_V > 0$ are valid for all materials. Similar versions of the pressure equation can be found in [6, 12].

### *2.4. Coefficients of differential susceptibility; first approximation*

Equation (22) is the general form of the pressure equation in which careful consideration of thermodynamic quantities has been made. However, we can introduce several simplifying assumptions on the experimentally measurable thermodynamic variables $\beta$, $\gamma$, $k$ and $c_p$. These quantities, in general, are not constants but functions of the thermodynamic state. By nature, they are coefficients of differential susceptibility: they tell us how, when we hold all variables but one fixed and deferentially "perturb the system", the solitary unconstrained variable responds. These coefficients all arise from perturbation processes that are by nature calorimetric. As a first approximation one can assume that they are temperature independent and thus taken to be constant. Under this assumption, (22) is shown to be

$$\frac{1}{K_S}\frac{dP}{dt} = -\boldsymbol{\nabla}\cdot\mathbf{u} + \frac{\alpha\beta}{k}\Phi + \gamma\alpha\boldsymbol{\nabla}\cdot\left(\frac{1}{K_S(P,T)}\boldsymbol{\nabla}P\right) - \alpha\boldsymbol{\nabla}\cdot\left(\frac{1}{\rho}\boldsymbol{\nabla}\rho\right) \quad (23)$$

noting that the adiabatic incompressibility modulus $K_S$ generally varies with pressure and temperature. If viscous dissipation effects are neglected, all that reamins for (23) to be useful is to develop models for only two thermodynamic properties; $K_S$ and $\alpha$, certainly a much simpler task.

## 3. Model Parameters

A more elaborate theoretical consideration is needed to make the proposed pressure equation useful. To this end, the modeling of $K_S$ is first made and then the estimation of $\alpha$ is briefly discussed.

### 3.1. Incompressibility modulus

While equation (22) must hold for any fluid flow, there are idealized situations in which this equation can be further simplified. The condition of zero thermal diffusivity $\alpha = 0$ results in the conservation of entropy $dS = 0$ and we say that the flow is isentropic. This is an idealized thermodynamic process that is adiabatic and in which work transfers are frictionless. The simplifying feature of isentropic flow is that exchanges between internal energy and other forms of energy are reversible, and the internal energy and temperature play passive roles; merely changing in response to the compression of a fluid.

The incompressibility modulus is, in general, dependent on both temperature and pressure[13], i.e. $K_S = K_S(T, P)$. By Taylor expanding around the reference thermodynamic state $\Omega_0 := (T_0, P_0)$:

$$K_S(P,T) = K_S(P,T)\Big|_{\Omega_0} + \frac{\partial K_S}{\partial P}\Big|_{\Omega_0}(P-P_0) + \frac{\partial K_S}{\partial T}\Big|_{\Omega_0}(T-T_0) + \frac{1}{2!}\frac{\partial^2 K_S}{\partial P^2}\Big|_{\Omega_0}(P-P_0)^2 + \frac{1}{2!}\frac{\partial^2 K_S}{\partial T^2}\Big|_{\Omega_0}(T-T_0)^2 + \dots \quad (24)$$

Assuming that temperature dependency is negligible or that $K_S$ varies weakly with temperature, then for a reference pressure $P_0 = 0$:

$$K_S(P) = K_{S,0} + \gamma P + \zeta P^2 \quad \text{with} \quad \gamma := \frac{\partial K_S}{\partial P}\Big|_{P=0}, \ \zeta := \frac{1}{2!}\frac{\partial^2 K_S}{\partial P^2}\Big|_{P=0} \quad (25)$$

where $K_{S,0}$ is the reference adiabatic incompressibility modulus at $P = 0$. The parameters $\gamma$ and $\zeta$ must, in general, be determined empirically. $K_S$ must increase with pressure and the simplest relationship satisfying this requirement is when $\zeta = 0$ and the resulting equation is sometimes known as Murnaghan's equation [13–15]. In the following analysis we first consider the two parameters $\gamma$ and $K_{S,0}$ and their use/definitions in SPH. For isentropic

flows, the thermal diffusivity is zero. This implies that the last 3 terms of (23) must vanish. In that case, the pressure equation reduces to a simple differential form were pressure is barotropic:

$$dP = (K_{S,0} + \gamma P)\frac{d\rho}{\rho}, \quad P|_{\rho=\rho_0} = 0, \quad K_{S,0} = \rho \frac{\partial P}{\partial \rho}\bigg|_{S,\rho=\rho_0} \tag{26}$$

which is an easily solvable differential equation. Equation (26) could be referred to as the integrated linear theory. A simple integration of the above equation yields the standard equation of state for SPH where the pressure varies non-linearly with the density:

$$P(\rho) = \frac{1}{\gamma} K_{S,0} \left[ \left( \frac{\rho}{\rho_0} \right)^{\gamma} - 1 \right] \tag{27}$$

This equation is called Murnaghan equation of state [13–15] and $\zeta = 0$ in this case. By further defining the reference adiabatic speed of sound $c^2_{s,0} := (\partial P/\partial \rho)_s|_{\rho=\rho_0}$ then it is easy to show that $K_{S,0} = \rho_0 c^2_{s,0}$. Note that for an ideal gas $K_{S,0} \equiv 0$ since $K_S = \gamma P$, which further yields the more familiar ideal gas equation of state $P(\rho) = A(s)\rho^{\gamma}$. Here $A(s)$ is the adiabat, itself a function of the entropy. In the case of isentropic flows, $s$ and thus $A$ remain constant.

### *3.2. The parameter $\zeta$*

In thinking about volume and temperature changes, we often have some sort of gas in mind. This is clearly the case in WCSPH, for instance, where liquids are modeled as gases. However, in fluid-fluid and fluid-structure impact flows we have to deal with very large pressures during impact where changes in volume and temperature are not negligible. One parameter that

could be useful in characterizing these types of flows is the Grüneisen parameter, a dimensionless property. Knopoff and Shapiro [16] showed that $\Gamma$ for water does become substantially independent temperature at high pressure. This lack of dependence of $\Gamma$ on $T$ for part of volume of water implies that techniques of lattice dynamics, originally developed for solids, can be applied to the liquid in this range. Under these conditions [16], the volume dependence of $\Gamma$ is given by

$$\Gamma(V) = \frac{t-2}{3} - \frac{V}{2}\frac{\frac{d^2}{dV^2}\left(PV^{\frac{2t}{3}}\right)}{\frac{d}{dV}\left(PV^{\frac{2t}{3}}\right)} \tag{28}$$

where the case $t = 2$ is called the free-volume (FV) formulation. The Slater-Landau (SL) and Dugdale-MacDonald (DM) formulations are obtained by setting $t = 0$ and $t = 1$, respectively. Using definitions (15) for the incompressibility modulus, we can rewrite equation (28) as

$$\Gamma(V) = -\frac{1}{6} + \frac{1}{2}\frac{K_S'(P) - \frac{2t}{3}}{1 - \frac{2t}{3}\frac{P}{K_S(P)}} \tag{29}$$

where adiabatic compressions are assumed and so the subscript $S$ is designated. Then from equation (25), we have $K_S' = \gamma + 2\zeta P$ and then $\Gamma_0$ is given by

$$\Gamma_0 = -\frac{1}{6} + \frac{1}{2}\left(\gamma - \frac{2t}{3}\right) \tag{30}$$

With the assumption that $\Gamma$ is independent of temperature, methods of lattice dynamics (specifically developed for solids where $\Gamma$ is nearly independent of $T$) are applicable to liquids as well [16]. Using these ideas, Mao [14] derives a formula for the composite parameter $K_{S,0}K_{S,0}''$ which we refine as

$$-K_{S,0}K_{S,0}'' = 2\Gamma_0\left(\Gamma_0 + \frac{1}{3}\right) + \frac{1}{3}\left(K_{S,0}' - \frac{1}{3}\right) \tag{31}$$

where $K'_{S,0} := (\partial K_S/\partial P)_{P=0}$, $K''_{S,0} := (\partial^2 K_S/\partial P^2)_{P=0}$ and $\Gamma_0 = \beta K_{S,0}/(\rho_0 c_p)$ is the reference Grüneisen number. Then from Eq. 25, we have $K'_{S,0} = \gamma$ and $K''_{S,0} = 2\zeta$. This leads to the following estimator for $\zeta$:

$$\zeta = -\frac{1}{2\rho_0 c_{s,0}^2}\left[\frac{1}{3}\left(\gamma - \frac{1}{3}\right) + 2\Gamma_0\left(\Gamma_0 + \frac{1}{3}\right)\right] \tag{32}$$

from which the physical meaning is now relatively clear. Note that $\zeta$ is stritly negative i.e. $\zeta < 0$ as shown by equation (32) since $\gamma > 1$ and $\Gamma_0 > 0$. This theoretical result is indeed supported by experimental measurements as pointed out by Stacey et al. [13]. It is associated with the curvature in the $K(P)$ vs $P$ curve. Clearly, as $\zeta < 0$, at high pressure $K_S$ can attain negative values which would violate mechanical stability due to which $\gamma > 1$ and $K_S > 0$. This polynomial representation of $K_S$ would therefore be useful if $K_S$ remains positive over the compression range. Mao [14] presents an alternative to (25) by making the assumption that

$$K_S \frac{\partial P}{\partial K_S} = a + bP \tag{33}$$

whose solution yields:

$$K_S := K_{S,0}\left(1 + \frac{b}{a}P\right)^{\frac{1}{b}}, \quad a = \frac{K_{S,0}}{\gamma}, \quad b = 1 - 2\frac{\zeta K_{S,0}}{\gamma^2} \tag{34}$$

Unless stated explicitly, for computational efficiency, the polynomial approximation (25) will be used by default.

### *3.3. Thermal diffusivity*

With regards to the thermal diffusivity, an assumption made in [6] is that the Prandtl number is approximated by $\mathrm{Pr} = \gamma$. Consequently, from

the formal definition of the Prandtl number i.e. $\text{Pr} := \frac{\nu}{\alpha}$, we obtain an estimator for the thermal diffusivity:

$$\alpha = \frac{\nu}{\gamma}. \tag{35}$$

Ramachandran and Puri [7] found that if the physical viscosity is used in the EDAC scheme, the system is unstable as pressure builds up quickly. They also report non-physical solutions when large values of the viscosity are used. Since the physical viscosity is not always suitable, they suggest using the artificial viscosity used in standard WCSPH schemes where

$$\nu_e = \frac{\lambda h c_{s,0}}{8} \tag{36}$$

where the parameter $\lambda$ was found to be $\lambda \approx 0.5$ for most simulations with Reynolds number in the range 0.0125 to $10,000$. It shall be made explicitly clear whenever this artificial viscosity $\nu_e$ is used in our simulations. Notably, this is the same idea adopted in the $\delta$-SPH scheme where the artificial diffusion coefficient in the continuity equation is modeled as $\delta h c_{s,0}$ and the parameter $\delta$ controls the magnitude of the diffusion term [5].

### *3.4. Summary*

In summary, the proposed artificial compressibility model $g$EDAC as the final formulation is given by

$$\frac{d\rho}{dt} = -\rho \boldsymbol{\nabla} \cdot \mathbf{u} \tag{37a}$$

$$\rho \frac{d\mathbf{u}}{dt} = -\boldsymbol{\nabla} P + \rho \nu \nabla^2 \mathbf{u} + \rho \boldsymbol{g} \tag{37b}$$

$$\kappa_s \frac{dP}{dt} = -\boldsymbol{\nabla} \cdot \mathbf{u} + \gamma \alpha \boldsymbol{\nabla} \cdot (\kappa_s(P) \boldsymbol{\nabla} P) - \alpha \boldsymbol{\nabla} \cdot \left( \frac{1}{\rho} \boldsymbol{\nabla} \rho \right) \tag{37c}$$

This system of equations is then closed by introducing the adiabatic incompressibility modulus model given by equation (25) or (34). The three parameters for the parameterization of the incompressibility modulus include the reference incompressibility modulus which determined by

$$K_{S,0} := \rho_0 c_{s,0}^2 \tag{38}$$

so that $K_{S,0}$ is known once the reference values for the density and sound speed are prescribed. The other two are $\zeta$ which is estimated from equation (32) and $\gamma$ whose values are well known in SPH. Consequently all the thermodynamic properties *viz.* $K_S$, $\alpha$ and $\zeta$ are fully determined as they are all functions containing only two thermodynamic constants; $\gamma$ and $K_{S,0}$. The nature of the parameter $\gamma$ is well understood within the SPH framework where $\gamma = 1.04$ for air and $\gamma = 7.0$ for water and in our model, we will adopt this same criteria for setting $\gamma$. This connection is due to (27) being the same as the standard equation of state that is widely used in SPH. In one sense, it can be argued that the meaning of $\gamma$ and $K_{S,0}$ is less ambiguous than that of $\zeta$.

## 4. Causality

It is important to discuss the numerical implications of the pressure equation model above. Explicit time stepping numerical methods, in general, have their own condition for causality called the CFL stability criterion. However, for highly viscous flows the time step is controlled by the viscosity. This viscous time step in SPH is given by $\Delta t \leq C_\nu \frac{h^2}{\nu}$ with $C_\nu = 0.125$. The stability criterion on the diffusion term in the pressure equation can be calculated

independently of the equations of motion since its stability is dependent on the thermal timescale rather than the dynamic timescale. In this case, the constraint on the timestep due to thermal diffusivity is given,

$$\Delta t \leq C_\alpha \frac{h^2}{4\gamma\alpha}, \qquad 0 < C_\alpha < 1 \tag{39}$$

where the parameter $C_\alpha$ depends on the dimensionality of the problem. In particular, under the assumption that $\nu \approx \gamma\alpha$, then $\Delta t \leq C_\alpha \frac{h^2}{4\nu}$. This corresponds to the constraint on the timestep due to viscous diffusion with $C_\alpha = \frac{1}{2}$ for most SPH schemes [17]. For a detailed derivation of (39), the interested reader can refer to Appendix B.

The pressure equation as presented above damps pressure oscillations via a thermal diffusion process. Therefore, this scheme is conceptually similar to the $\delta-$SPH approach where diffusive terms are artificially introduced into the continuity equation, albeit in a rather heuristic manner. The smoothed density is then used to compute a smooth pressure from the equation of state (2), see Antuono et al. [5] for details.

## 5. Discretization

The implementation of the generalized EDAC or $g$EDAC scheme follows the work in [7] on the EDAC scheme. The diffusion terms in the pressure equation are, however, implemented according to [18]. In Standard SPH schemes a fluid is treated as quasi-incompressible, i.e. the weakly compressible SPH. Here the density is dynamically evolved by the discretized continuity equation or the density summation interpolant [19]. The other class of SPH schemes comprise fully incompressible SPH schemes or ISPH and its

variants. In the ISPH approach the density is constant whereas the pressure is obtained by solving the Poisson pressure equation. For the EDAC scheme the density can either be held constant or evolved. Caution, however, that for flows involving liquid-solid impacts it is probably best to solve the continuity equation and the pressure equation separately. For these kinds of problems the pressure value is of particular importance especially in practical applications [5]. Doing things this way could ensure that smooth density enters the pressure and momentum equations for a smooth solution. In this work, we use the density summation approach to compute the density.

Using the number density approach [5], the momentum equation becomes:

$$\frac{d\mathbf{u}_i}{dt} = \frac{1}{m_i}\sum_{j=1}\left(V_i^2 + V_j^2\right)\left\{-\widetilde{P}_{ij}\boldsymbol{\nabla}w_{ij} + \widetilde{\eta}_{ij}\mathbf{u}_{ij}\frac{\mathbf{r}_{ij}\cdot\boldsymbol{\nabla}w_{ij}}{\|\mathbf{r}_{ij}\|^2 + \epsilon h^2}\right\} + \boldsymbol{g}_i \tag{40}$$

where the relative position $\mathbf{r}_{ij} := \mathbf{r}_i - \mathbf{r}_j$, relative velocity $\mathbf{u}_{ij} := \mathbf{u}_i - \mathbf{u}_j$, smoothing length $h$ and $\epsilon h^2$ is a softening parameter to prevent divergence due to two interacting fluid particles being very close together. Typically the value $\epsilon = 0.01$ is chosen.

$$V_i = \frac{1}{\sum_j w_{ij}}, \qquad \widetilde{\eta}_{ij} = \frac{2\eta_i\eta_j}{\eta_i + \eta_j}, \quad \widetilde{P}_{ij} = \frac{\rho_j P_i + \rho_i P_j}{\rho_i + \rho_j} \tag{41}$$

with dynamic viscosity $\eta_i = \rho_i\nu_i$. Similarly, the equation for pressure:

$$\begin{aligned}\kappa_i\frac{dP_i}{dt} = &\sum_{j=1}\frac{m_j}{\rho_j}\mathbf{u}_{ij}\cdot\boldsymbol{\nabla}w_{ij} + \gamma\alpha\sum_{j=1}\frac{1}{m_i}\left(V_i^2 + V_j^2\right)\widetilde{\kappa}_{ij}P_{ij}\frac{\mathbf{r}_{ij}\cdot\boldsymbol{\nabla}w_{ij}}{\|\mathbf{r}_{ij}\|^2 + \epsilon h^2} \\ &- \alpha\sum_{j=1}\frac{1}{m_i}\left(V_i^2 + V_j^2\right)\rho_{ij}\frac{\mathbf{r}_{ij}\cdot\boldsymbol{\nabla}w_{ij}}{\|\mathbf{r}_{ij}\|^2 + \epsilon h^2}\end{aligned} \tag{42}$$

where $P_{ij} := P_i - P_j$ is the relative pressure and $\rho_{ij} := \rho_i - \rho_j$ is relative density.

$$\rho_i = \frac{m_i}{V_i}, \quad \kappa_i = \frac{1}{\rho_0 c_{s,0}^2 + \gamma P_i + \zeta P_i^2}, \quad \widetilde{\kappa}_{ij} = \frac{2\rho_i\kappa_i\cdot\rho_j\kappa_j}{\rho_i\kappa_i + \rho_j\kappa_j} \tag{43}$$

The particles are then moved according to

$$\frac{d\mathbf{r}_i}{dt} = \mathbf{u}_i \tag{44}$$

Only 2D simulations are considered in this paper. The kernel of choice is the quintic spline $w_{ij} := w(\|\mathbf{r} - \mathbf{r}'\|, h)$:

$$w(q) = \alpha_2 \begin{cases} (3-q)^5 - 6(2-q)^5 + 15(1-q)^5, & 0 \le q \le 1 \\ (3-q)^5 - 6(2-q)^5, & 1 \le q < 2 \\ (3-q)^5, & 2 \le q < 3 \\ 0, & q \ge 3 \end{cases} \tag{45}$$

where the normalization constant $\alpha_2 = 7/(478\pi h^2)$ and the normalized relative position $q = \|\mathbf{r}_{ij}\|/h$. Unless otherwise stated, the quintic spline will be used in all simulations.

The predictor-corrector time integration scheme described in [7] is used to integrate the equations (40) and (42). The implementation of the EDAC and our proposed $g$EDACscheme follow the work of Ramachandran and Puri [7].

## 6. Model validation

The generalized EDAC model, $g$EDAC for short, is used to test a number of benchmark problems in the SPH framework. Comparisons are made with EDAC scheme [7]. The code for the $g$EDAC is implemented within the open source code developed by Ramachandran and Puri [7].

### 6.1. Couette and Poiseuille Flows

The first two test cases to be considered here are the Poiseuille flow and the Couette flow in a 2D infinite dimensional channel where the walls are separated by $L_y = 1\,\mathrm{m}$. The physical properties of the fluid are specified as; viscosity $\nu = 0.01\,\mathrm{m\,s^{-2}}$ and density $\rho = 1.0\,\mathrm{kg\,m^{-3}}$. The fluid is dicretized with SPH particles having initial particle spacing $\Delta x = 0.05\,\mathrm{m}$. Periodicity is imposed in the $x$-direction and we only simulate a small section of width $L_x = 0.4L_y$. In either test case, the maximum velocity $u_{\max} = F_x d^2/(2\mu) = 1.25\,\mathrm{m\,s^{-1}}$ with the driving force for the Poiseuille flow $F_x = 0.1\,\mathrm{N}$ and $d = 0.5L_y$. For the Couette flow the upper plate is moved with a constant velocity of $u_w = 1.25\,\mathrm{m\,s^{-1}}$. The artificial sound speed is taken to be the standard SPH choice of $c_{s,0} = 10u_{\max}$.

Fig. 1a shows a comparison of the $g$EDAC simulation with the analytical solution for the Poiseuille flow at times $t = 2\,\mathrm{s},\ 10\,\mathrm{s},\ 20\,\mathrm{s}$ and $100\,\mathrm{s}$. The observations indicate good consistency with the expected physical phenomena; initially the fluid is at rest but gets accelerated by the driving force. At steady state, parabolic velocity profiles develop and the solution converges to the analytical solution at large $t$.

The $g$EDAC simulation is compared with the analytical solution for the Couette flow at times $t = 2\,\mathrm{s},\ 10\,\mathrm{s},\ 20\,\mathrm{s}$ and $100\,\mathrm{s}$, and the result is shown in fig. 1b. There is good agreement between the simulated profiles and the analytical solutions and convergence is achieved for large $t$.

### 6.2. Hydrostatic test

The goal of this test case is to establish how well the proposed pressure equation evolves the pressure. The setup for this simulation is from Adami

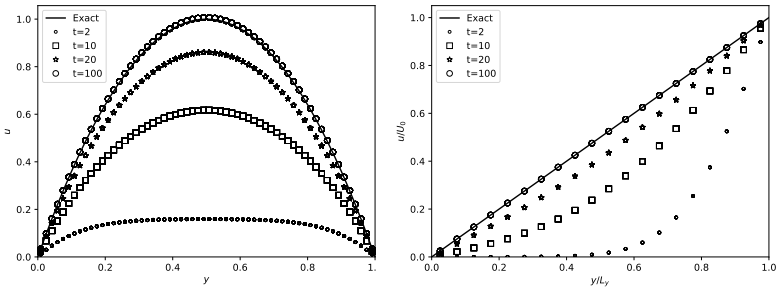


(a) Poiseuille (b) Couette

Figure 1: Comparison of the $g$EDAC simulation with the analytical steady solution for the Poiseuille flow (a) and the Couette flow (b).

et al. [20] where a $2\,\mathrm{m} \times 1\,\mathrm{m}$ tank is filled with water up to a height $H = 0.9\,\mathrm{m}$. Recently, Ramachandran and Puri [7], Hu et al. [21] among others, have also used the same setup. The top of the tank is left open and the fluid is initialized with zero pressure and velocity fields. The reason for this choice of initial condition is that although an exact solution of the Navier-Stokes equations exists for this problem, one would ideally initialize the pressure as $p_i = \rho_0 g(H - y_i)$ for each fluid particle. However, this is not generally suitable as the SPH particles come to equilibrium due to the effect of boundary forces and gravity [22].

The adiabatic incompressibility modulus $K_s$ defined by (38) is parameterized with $\gamma = 7.0$, and $\lambda = 0.5$. The rest density of water is $\rho_0 = 1000\,\mathrm{kg\,m^{-3}}$, and acceleration due to gravity is set at a lower value of $g = -1.0\,\mathrm{m\,s^{-2}}$. The artificial sound speed was taken to be ten times the reference velocity $U = \sqrt{gH}$. As discussed in [7, 20] artificial viscosity with the parameter $\alpha_v = 0.24$ corresponds to a Reynolds number $Re = 100$ and no physical viscosity is used.

The particles are initially placed on a rectangular grid with inter-particle spacing set at $\Delta x = \Delta y = 0.02\,\mathrm{m}$ with $h = 1.2\Delta x$. For this configuration, this implies a total of $100 \times 50 = 5000$ particles. This is obviously not an equilibrium state and due to a jump in the initial data resulting from a response to gravity and boundary forces, spurious high frequency pseudo-sound waves travel through the domain. In this work such artificial effects are damped using the model suggested by Monaghan and Kajtar [22] and explicit details are given by Adami et al. [20]. The boundary conditions on the solid walls are free-slip whereas the dynamic free surface boundary condition is not imposed, as is the case for SPH. The problem is simulated for the EDAC and $g$EDAC schemes.

A plot of the pressure at the bottom of the tank is as shown in Fig. 2. Since the system is not initially in hydrostatic equilibrium, in response to gravity at $t = 0^+$, the system begins to readjust to hydrostatic equilibrium in an oscillatory mode. Particularly, the EDAC scheme of Ramachandran and Puri [7] tends to produce a pressure field that is quite oscillates . On the other hand, the $g$EDAC model shows less oscillations than the EDAC scheme for $\zeta = -0.03\,\mathrm{Pa}^{-1}$. In particular, when $\zeta = 0$, the $g$EDAC scheme shows a stable pressure field that shows small oscillations. However, when $\zeta = -0.03$ the $g$EDAC has less oscillations in the pressure field than both the EDAC. This improvement is attributable to the quadratic term $\zeta p^2$ in the incompressibility modulus given by equation (38).

Fig. 3 shows the variation of pressure $p_i = p(y_i)$ at the center of the tank for the two schemes. Like the EDAC scheme, the $g$EDAC produces an accurate pressure distribution.

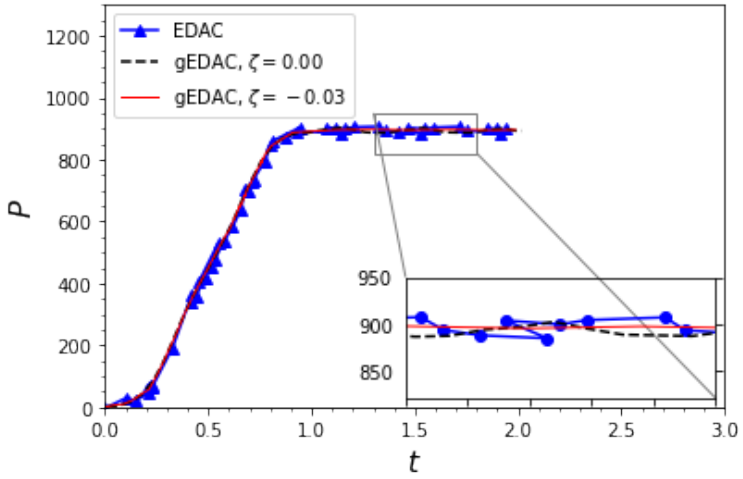


Figure 2: Plot of the pressure at the bottom of the tank versus time for different schemes.

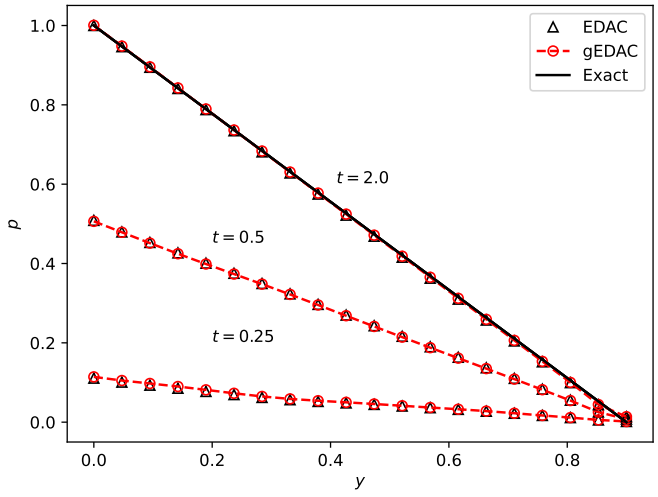


Figure 3: Pressure variation with height for the two schemes at $t = [0.25, 0.5, 2.0]$.

### *6.3. Impinging water jets in 2D*

This is a recent addition to the standard benchmark tests for SPH schemes [23]. The impact of two rectangular, identical water jets each of length $L$ and width $2H$ at time $t = 0^+$ when they form an interface at $y = 0$ is considered. The upper jet moves down the $y$-axis with velocity $v = -U$ whereas the lower jet moves in the opposite direction with velocity $v = +U$. No external forces are applied and the flow is assumed to be incompressible and inviscid. In their study, Marrone et al. [23] used a fully incompressible Riemann-SPH solver whereas Ramachandran and Puri [7] used the EDAC scheme and also the WCSPH. Here we only compare the EDAC scheme with our proposed $g$EDAC scheme. For this test case $L = 1.0\,\mathrm{m}$, $H = 2.0\,\mathrm{m}$, $U = 1.0\,\mathrm{m}$ and $\rho = 1.0\,\mathrm{kg\,m^{-3}}$. Variations in density are restricted to be on the order of $0.01\,\%$ by fixing the Mach number at $\mathrm{Ma} = 0.01$. The smoothing kernel for all three cases is a quintic spline with smoothing length $h = \Delta x$ and $L/\Delta x = 100$. Furthermore, for this test case the incompressibility modulus of Mao [14] (given by equation (34) above) is used and $\gamma = 7.0$ and $\lambda = 0.8$. The simulations were performed with artificial viscosity parameter $\alpha_v = 0.1$. This leads to a stabilized pressure field. Both the EDAC scheme Fig. 4 and $g$EDAC scheme Fig. 5 tend to produce less oscillatory pressure fields/velocity fields. Results from both schemes are comparable with those obtained from the SPH-Riemann solver of Marrone et al. [23].

### *6.4. Fluid-fluid and fluid-structure impacts generated by a dam-break*

Now we consider the dam-break problem studied by Marrone et al. [24]. This is a standard benchmark free-surface problem that involves the collapse of a water column. The water column is of height $H = 0.6\,\mathrm{m}$ and width

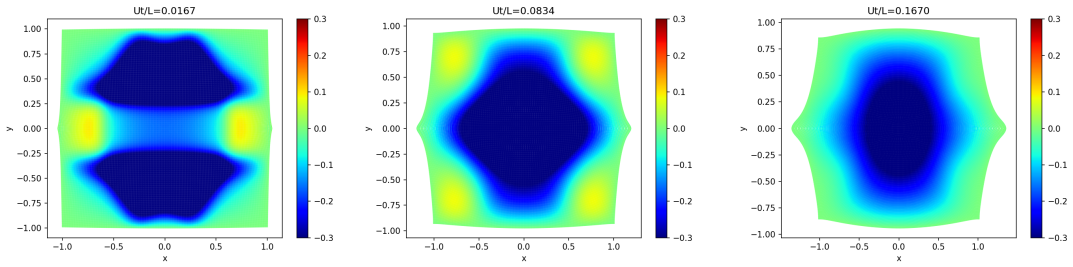


Figure 4: Particle distribution and pressure at times $Ut/L = [0.0167$ (left) and $Ut/L = 0.167$ (right) for simulation with the standard EDAC scheme with artificial viscosity coefficient $\lambda = 0.8$.

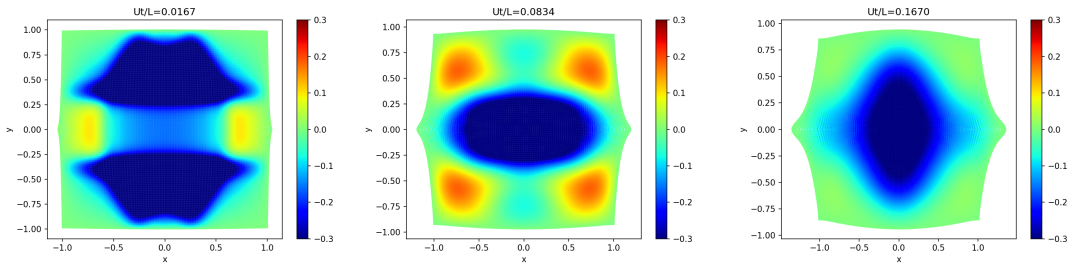


Figure 5: Particle distribution and pressure at times $Ut/L = [0.0167$ (left) and $Ut/L = 0.167$ (right) for simulation with the standard EDAC scheme with artificial viscosity coefficient is 0.8.

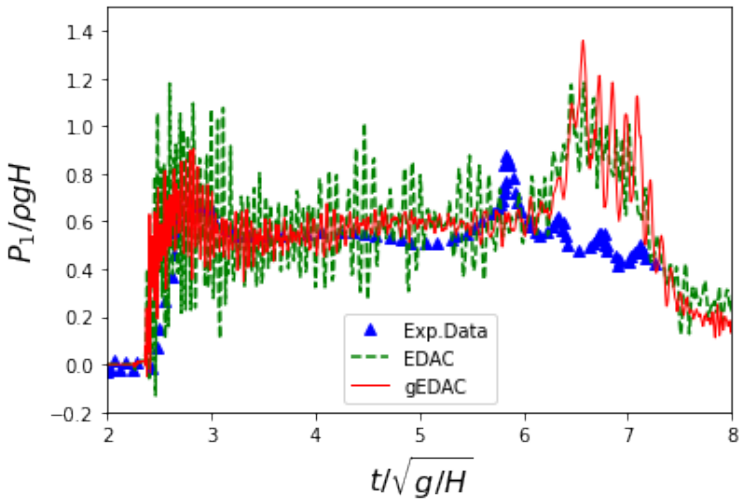


Figure 6: Comparison of the temporal pressure profiles at probe $P_1$: 0.16 m between experimental data [25], EDAC and $g$EDAC simulations with $H/\Delta x = 75$.

$L = 2H$. The container has width $L_w = 5.366H$ and we set its height at $H_w = 2.0\,\mathrm{m}$. Fluid particles are uniformly distributed as [7] with initial particle spacing $\Delta x = 0.008\,\mathrm{m}$ and smoothing length $h = 1.2\Delta x$. The two correction schemes of XSPH and artificial viscosity are not employed in this simulation. The fluid has density $\rho_0 = 1000\,\mathrm{kg\,m^{-3}}$ and the speed of sound is given by $c_{s,0} = 10\sqrt{2gH}$. The artificial diffusion parameter of 0.5 is used for the EDAC scheme. Following the suggestion of Ramachandran and Puri [7], the boundary pressure is clamped to non-negative to prevent it from sticking to the walls. For the gEDAC scheme the parameters for the incompressibility modulus $\gamma = 7$ is used.

For a quantitative validation, the temporal pressure on the downstream wall at the probe $P_1 : y = 0.16\,\mathrm{m}$ is compared with experimental data from

Buchner [25]. A naive method

$$P_1(t) = \frac{1}{N(t)} \sum_{i=1}^{N(t)} P_i(t)$$

was used to interpolate the pressure at the probe. Here $N(t)$ is the number of fluid particles within a fixed distance of 0.09 m from the probe at time $t$. Both the EDAC and $g$EDAC schemes agree with the experiment up to about $t\sqrt{g/H} = 5.8$. The peak at $t\sqrt{g/H} = 6.0$ is due to the the plunging wave of the first roll-up when the flow hits the right wall. There is a delay in the occurrence of the first peak as the effect of air-entrapment is not taken into account in our simulations; a two-phase flow is needed to capture this effect. For the same spatial resolution, the EDAC scheme exhibits higher oscillations than the $g$EDAC scheme. The EDAC scheme approximates the incompressibility modulus as simply $K_S = \rho c_{s,0}^2$ whereas the $g$EDAC employs a higher order approximation to account for high-pressure effects.

Fig. 7 shows snapshots of the dam-break simulation at times $t = 0.4\,\mathrm{s}$, $0.8\,\mathrm{s}$, $1.4\,\mathrm{s}$ and $1.6\,\mathrm{s}$. The snapshots capture the time evolution of the dam-break flow up to generation of a cavity at $t = 1.6\,\mathrm{s}$. The results are in good agreement with those of Marrone et al. [24]. Fig. 8 displays similar snapshots for the EDAC scheme.

### *6.5. Lid-driven-cavity*

This problem constitutes a very good test for a numerical scheme's capability to simulate viscous flows. The fluid domain is a $1.0\,\mathrm{m} \times 1.0\,\mathrm{m}$ box containing a fluid whose rest density is $\rho_0 = 1.0\,\mathrm{kg\,m^{-3}}$. No-slip boundary conditions are imposed at the walls except for the top wall which is a moving boundary at a uniform velocity $u_w$. With the Reynolds number given

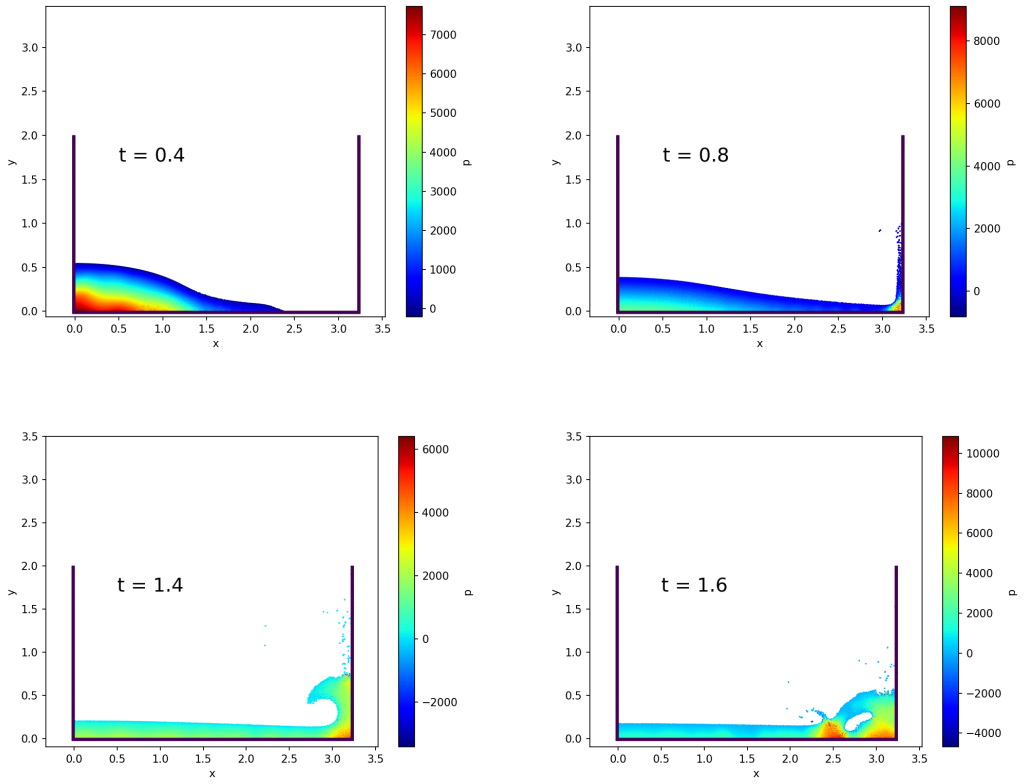


Figure 7: snapshots of the dam-break simulation for the $g$EDAC scheme

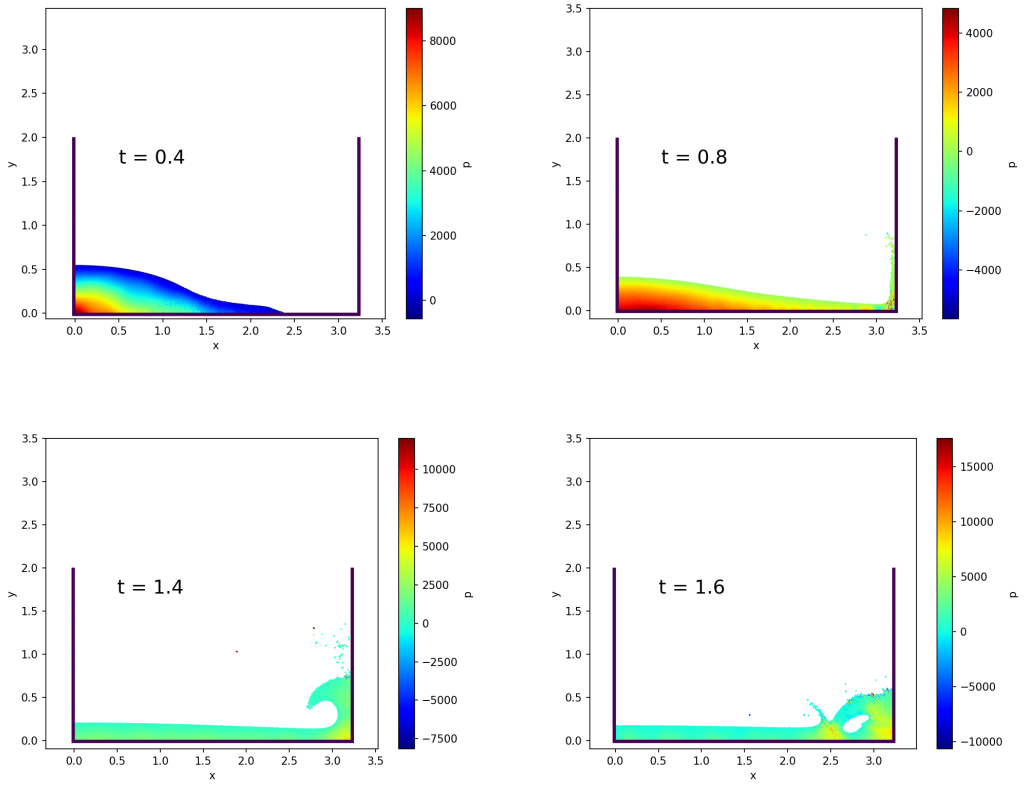


Figure 8: snapshots of the dam-break simulation for the EDAC scheme

by $Re = u_w/\nu$, laminar flow in the cavity was investigated for $Re = 100$ and $Re = 1000$ [7]. An interesting feature of this problem is that while the geometry is very simple, no known analytical solution exists. Two singularities emerge at the top corners due to the moving lid on the top horizontal wall boundary and the no-slip conditions on the vertical wall boundaries [26]. It therefore presents one of the well-known challenging test cases for SPH schemes and as such it is customary to validate against reference data from a numerical calculation performed on a fine grid by Ghia et al. [27]. Here, simulation results from the EDAC scheme and the $g$EDAC scheme are compared with this reference data.

The quintic spline with smoothing length $h = \Delta x$ was used and the fixed time-step predictor-corrector scheme was used for the integration. For the $g$EDAC scheme the parameter $\gamma = 1.04$ is used. The fluid particles are assigned a density $\rho_0$ =1.0 kg m$^{-3}$ and were initially uniformly distributed on a $50 \times 50$ rectangular grid for $Re = 100$ and $100 \times 100$ for $Re = 1000$ [7]. Results are presented for comparatively low resolutions to highlight the gains available due to a generalized incompressibility (bulk) modulus in the $g$EDAC scheme compared with standard EDAC [7]. Both the EDAC and $g$EDAC simulation results agree well with the results of [27] and the same conclusion was reached by Ramachandran and Puri [7] even for low resolutions. There are noticeable improvements in the overlap between the $g$EDAC results and the benchmark solution [27]. This improvement can be further harnessed once a proper understanding of the empirical parameters $\gamma$ and $\zeta$ is established [13, 14, 28]. The results are in good agreement with the benchmark solution of Ghia et al. [27].

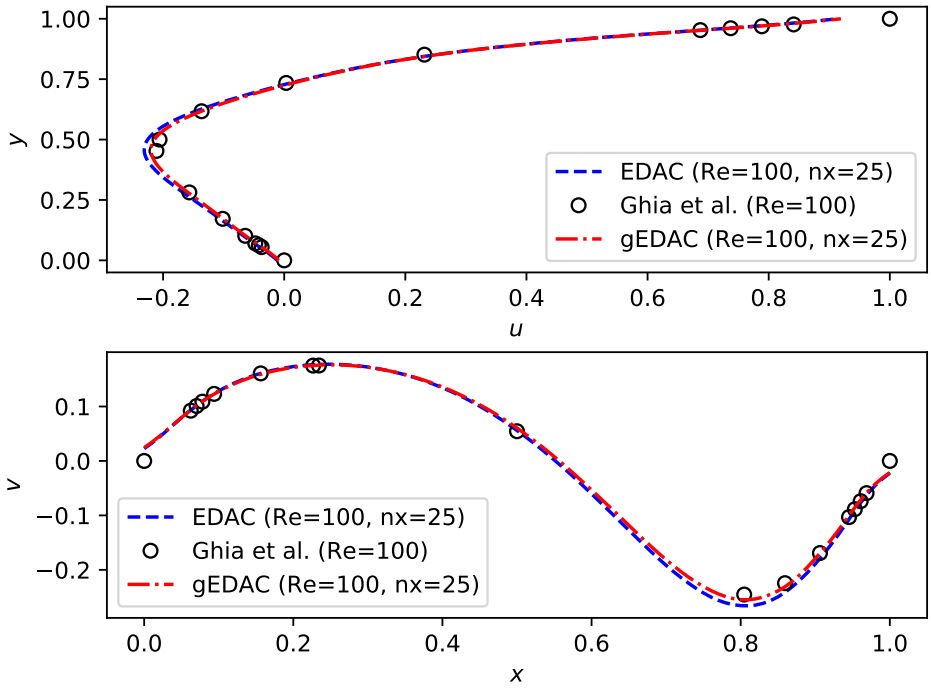


Figure 9: Horizontal velocity profile (top) and vertical velocity (bottom) vs $y$ for the lid-driven-cavity problem at $Re = 100$ with EDAC and $g$EDAC schemes. The results are compared with those of Ghia et al. [27].

Fig. 9 and Fig. 10 show the results for two resolutions at Reynolds numbers $Re = 100$ and $Re = 1000$, respectively. These results are in good agreement with those of Ghia et al. [27].

### *6.6. Taylor Green vortex*

The Taylor-Green vortex problem is widely used as a benchmark test for the numerical stability of smoothed particle hydrodynamics schemes. The viscous Taylor-Green vortex flow is a periodic array of vortices that is an

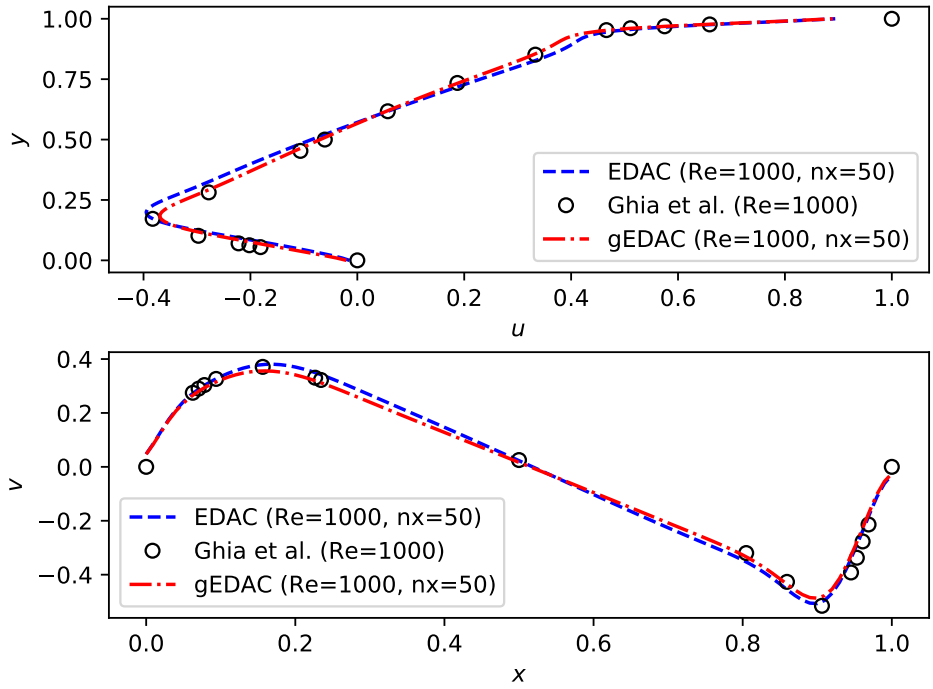


Figure 10: Horizontal velocity profile (top) and vertical velocity (bottom) vs $x$ for the lid-driven-cavity problem at $Re = 1000$ with EDAC and $g$EDAC schemes. The results are compared with those of Ghia et al. [27].

exact solution to the Navier-Stokes equations over a periodic domain and is given by

$$u(x, y, t) = -Ue^{bt} \cos(2\pi x) \sin(2\pi y) \tag{46a}$$

$$v(x, y, t) = Ue^{bt} \sin(2\pi x) \cos(2\pi y) \tag{46b}$$

$$p(x, y, t) = -\frac{1}{4} U^2 e^{2bt} [\cos(2\pi x) + \cos(2\pi y)] \tag{46c}$$

where the decay rate of the velocity field is given by $b = -8\pi^2/Re$; the Reynolds number $Re = UL/\nu$ is obtained from the maximum initial veloc-

ity $U = 1.0\,\mathrm{m\,s^{-1}}$ and the length of the periodic vortex array $L = 1.0\,\mathrm{m}$. The setup for this problem is as described in Adami et al. [26] and the same setup has been reproduced most recently by Ramachandran and Puri [7], Zhang et al. [29] among others. The fluid domain is a $1.0\,\mathrm{m} \times 1.0\,\mathrm{m}$ square with periodic boundary conditions. The artificial speed of sound is set by the standard SPH idea $c_0 = 10U$. The quinitic spline with $h$ set to the initial particle separation is used to run the simulation. For the two schemes:EDAC and $g$EDAC, no artificial viscosity was used as the physical viscosity is significant enough to generate smooth solutions [7]. The initial flow field $\{u(x, y, 0), v(x, y, 0), p(x, y, 0)\}$ is obtained from the exact solution above and the initial Reynolds number is set to 100.

Fluid particles are initially uniformly distributed with a small uniform random displacement superimposed onto the particles. The uniformly distributed random displacement in the $x$- and $y$-directions has a maximum value set at $0.2\Delta x$. All the schemes used in this problem were subjected to the same set of initial conditions.

In Fig. 11 the decay of the maximum velocity for different schemes is benchmarked against the exact solution. It is clear that the EDAC and $g$EDAC schemes perform relatively well. For this particular test, the gain in using the $g$EDAC scheme over the EDAC scheme is not obvious and this lack of distinction in accuracy applies to all schemes. As proposed in [7], the $L_1$ error is introduced as a better measure of performance between the two schemes. The $L_1$ error is defined as the mean value of the exact and numerical value of the absolute value of the velocity:

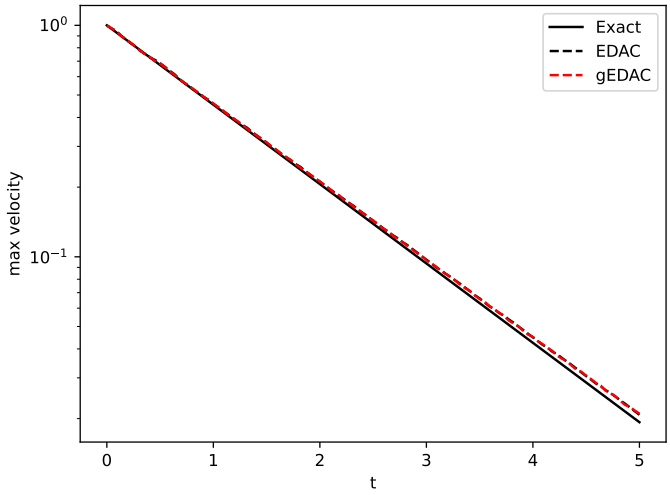


Figure 11: Variation of the velocity magnitude with time for the two schemes. Particles are initialized with $n_x = n_y = 50$ and thereafter randomly perturbed. The Reynolds number is chosen to be $Re = 100$. The quintic spline kernel is used with a smoothing length equal to the initial (undisturbed) particle spacing.

$$L_1 = \frac{\sum_i |\mathbf{u}_{i,\text{numerical}}| - |\mathbf{u}_{i,\text{exact}}|}{|\mathbf{u}_{i,\text{exact}}|} \tag{47}$$

where the value of $\boldsymbol{u}$ is computed at the positions for the $i^{\text{th}}$ particle in the flow.

From Fig. 12 it is evidently clear that the $g$EDAC and EDAC schemes produce comparatively the same result.

The most attractive feature of the EDAC and $g$EDAC schemes is that they can produce a smoother and stable pressure field than standard SPH schemes. To highlight this feature the time evolution of the $L_1$ error of the pressure field is given in Fig. 13. The $L_1$ error for the pressure field is defined

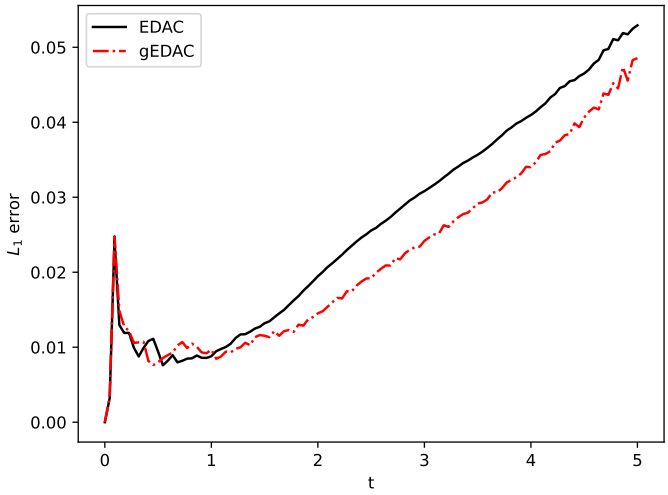


Figure 12: The time variation of the $L_1$ error for the velocity magnitude for the exact (black solid line), EDAC (black dash), $g$EDAC (red dash) schemes.

as:

$$p_{L_1} = \frac{\sum_i |p_{i,\text{numerical}} - p_{i,\text{exact}}|}{\max(p_{i,\text{exact}})} \tag{48}$$

The first observation from Fig. 13 is that the EDAC and $g$EDAC are comparable upto $t = 2s$, thereafter the $L_1$ for the EDAC scheme begins to grow and shows a nearly constant trend for the $g$EDAC scheme. The effect arising from the generalization of the EDAC on the computed pressure field is made manifest this test case.

The density summation formula is used in both the EDAC and $g$EDAC schemes implementations. The time evolution of the variation in the density computed using the summation density [7] is shown in Fig. 14 and serves as a test of how well the schemes preserve volume. The results for both schemes are comparable.

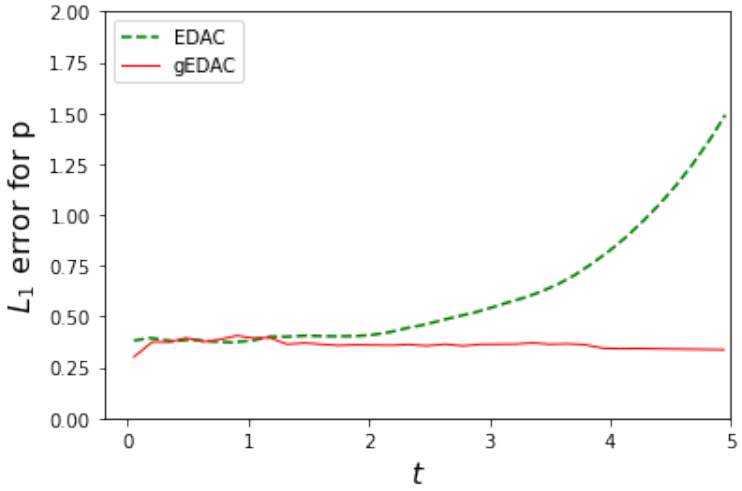


Figure 13: Time evolution of the $L_1$ error of the pressure field for the EDAC (green dash), $g$EDAC (red solid line) schemes.

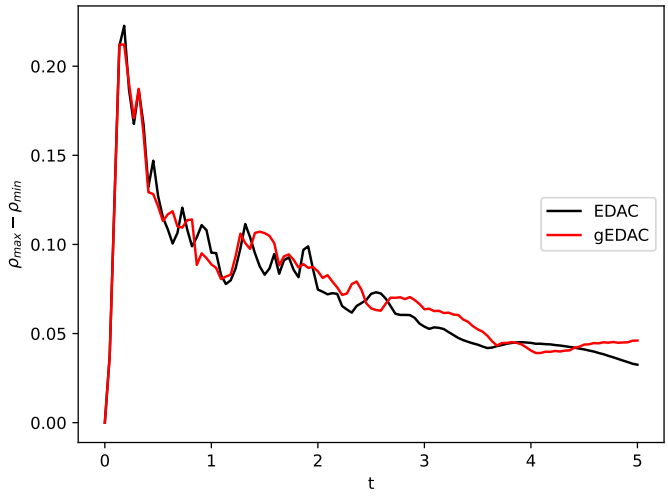


Figure 14: Time evolution of the density computed using the summation density for both the EDAC and $g$EDAC schemes. The number of particles is $n = 50 \times 50$ and $Re = 100$.

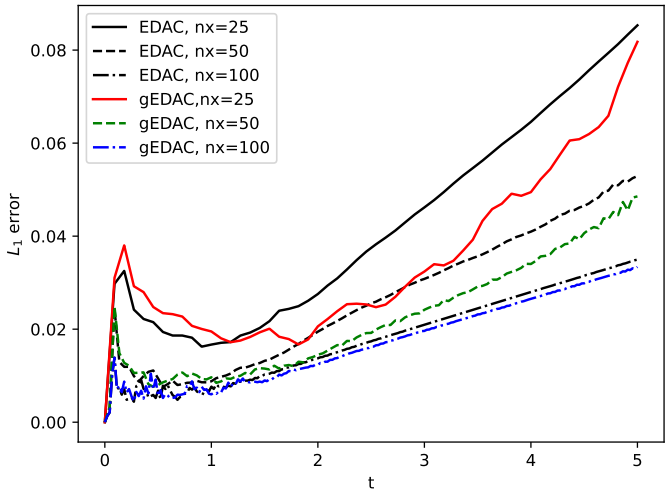


Figure 15: The $L_1$ error of the velocity magnitude versus $t$ for different resolutions.

We next consider the $L_1$ error of the velocity magnitude for different values of $n_x$ where the initial particle spacing is given by $\Delta x = 1.0/n_x$. Fig 15 shows that the $g$EDAC scheme produces a slightly smaller error than the EDAC scheme for the low resolutions considered.

The sensitivity the simulations to changes in the artificial thermal diffusivity parameter $\lambda$ is investigated by varying $\lambda$ for Re $= 100$ and $n_x = 25$. From fig. 16 it seems that a $\lambda$ value of 1.0 is reasonable. We perform a similar study with $Re = 10000$ with a higher particle resolution and present the results in Fig. 17. From both these cases it seems that using a$\lambda$ 1.0 is reasonable. In Fig. 17 Re $= 10000$ with $n_x = 101$ and $\lambda$ is varied. It seems plausible that $\alpha$ should be treated as an artificial parameter.

A convergence study at Re $= 1000$ for different $n_x$ is shown in Fig. 18. Convergence in the $L_1$ norm for the velocity magnitude can be seen in Fig. 18.

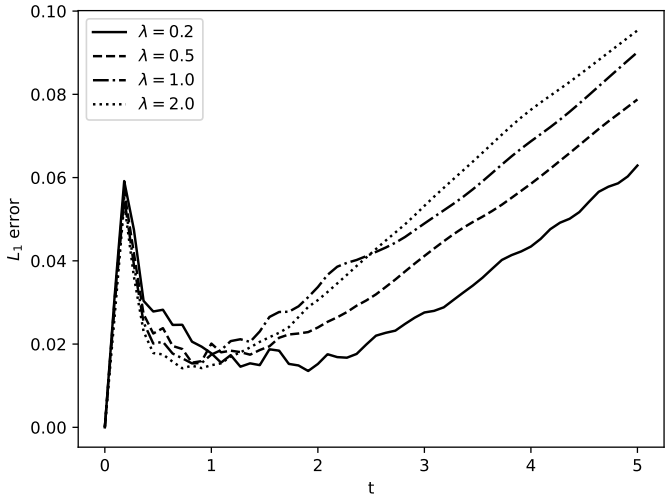


Figure 16: The $L_1$ error of the velocity magnitude versus $t$ for different choices of $\lambda$ with $Re = 100, n_x = 25$ while using the $g$EDAC scheme.

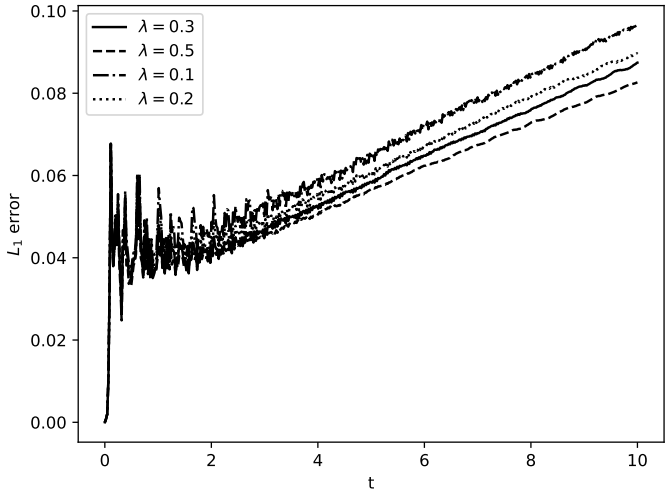


Figure 17: The $L_1$ error of the velocity magnitude versus $t$ for different choices of $\lambda$ at $Re = 10000$ while using the EDAC scheme. When $\lambda = 0$ is used the $\nu_{edac}$ is set to the fluid viscosity $\nu$.

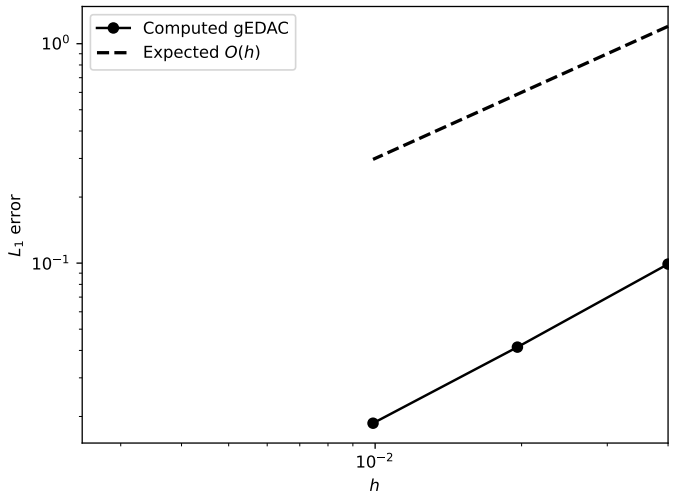


Figure 18: The $L_1$ error of the velocity magnitude at $t = 5$ versus $h$ at $Re = 1000$ for the EDAC scheme. The dashed line shows the convergence of an ideal scheme with first order convergence.

The $g$EDAC seems to exhibit first order convergence. Within the limits of SPH convergence, the scheme appears to be accurate. The known convergence issues with standard SPH still persist here. In particular the rate of convergence decreases with increased $n_x$. It is well known that for large $n_x$, convergence is only attained by also increasing $h$.

The above tests show that the $g$EDAC scheme is working correctly. Since $K_{S,0}$ is treated as an artificial parameter in SPH, it seems plausible that $\alpha$ must as well be treated as an artificial thermal diffusivity.

## 7. Conclusions

This paper investigated the generalization of the EDAC method of Clausen [6] in the weakly compressible context and its application to SPH. As such,

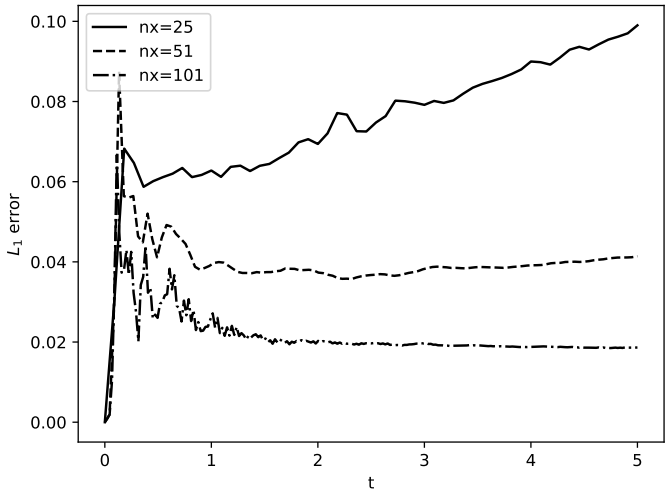


Figure 19: The $L_1$ error of the velocity magnitude versus $t$ for different choices of $n_x$ at $Re = 1000$ while using the $g$EDAC scheme.

the proposed method is applicable outside the domain of SPH. The $g$EDAC was implemented into the EDAC scheme developed by Ramachandran and Puri [7]. The gEDAC scheme performs better than the EDAC fluid flows involving impact. The $g$EDAC scheme shows improvements in the capture of the negative pressure region formed by two impinging jests and is consistent with results from Marrone et al. [23]. Similar, but slight, improvements in the $g$EDAC scheme over the EDAC scheme are observed for the lid-driven cavity problem and the Taylor-Green vortex problem. For some other cases, however, the difference between the EDAC and $g$EDAC scheme is hard to discern. Methods for determining the parameters $\alpha$, and $\zeta$ whereas $\gamma = 1.04$ for air and $\gamma = 7.0$ for water. In particular, our short analysis of the causality associated with pressure equation presented in this paper shows that there

is a condition on the time step; the thermal time step. Depending on the Prandtl number either the viscous time step or the thermal time step become more significant than the CFL conditions. This is possibly the reason why Ramachandran and Puri [7] reported non-physical solutions when physical viscosity is used in the pressure equation since using the physical viscosity imposes a prohibitively small time step. Ramachandran and Puri [7] instead proposed a heuristic expression based on the artificial viscosity and we similarly introduce the approximation $\gamma\alpha \approx \nu$ under the assumption that $Pr \approx \gamma$. A method for estimating $\zeta$ is also provided.

## 8. Acknowledgements

This work was supported by Okinawa Institute of Science and Technology Graduate University.

The implementation of the code in this work was realized in PySPH [30] due to its flexibility in implementing new equations to the existing ones. The code is publicly available at https://gitlab.com/pypr/edac_sph

## Appendix A. Maxwell's relations

The four Maxwell's relations are give by

$$\left(\frac{\partial T}{\partial V}\right)_S = -\left(\frac{\partial P}{\partial S}\right)_V \tag{A.1}$$

$$\left(\frac{\partial T}{\partial P}\right)_S = +\left(\frac{\partial V}{\partial S}\right)_P \tag{A.2}$$

$$\left(\frac{\partial S}{\partial V}\right)_T = +\left(\frac{\partial P}{\partial T}\right)_V \tag{A.3}$$

$$\left(\frac{\partial S}{\partial P}\right)_T = -\left(\frac{\partial V}{\partial T}\right)_P \tag{A.4}$$

## Appendix B. Causality

The stability criterion on the diffusion term in the pressure equation can be calculated independently of the equations of motion since its stability is dependent on the thermal timescale rather than the dynamic timescale. Thus, the pressure equation now reads;

$$\frac{dp}{dt} = \gamma\alpha\nabla^2 p \tag{B.1}$$

for a simple case of nearly constant adiabatic compressibility. We have further assumed that density gradients and thermal dissipation contributions are negligible. Consider a numerical fluctuation around a homogeneous state corresponding to the fluid equilibrium, i.e. $\rho(\mathbf{r}) = \bar{\rho}$ and $p(\mathbf{r}) = \bar{p}$. If the system is now perturbed from equilibrium, we have

$$\mathbf{r} = \bar{r} + \delta\mathbf{r}$$

$$\rho(\mathbf{r}) = \bar{\rho} + \delta\rho(\mathbf{r})$$

$$p(\mathbf{r}) = \bar{p} + \delta p(\mathbf{r})$$

Using the SPH approximation of the Laplacian operator, one obtains [1]:

$$\frac{d}{dt}\delta p(\mathbf{r}) = 2\gamma\alpha \int_\Omega (\delta p(\mathbf{r}) - \delta p(\mathbf{r}')) \frac{(\mathbf{r}-\mathbf{r}')\cdot\boldsymbol{\nabla} w_h}{\|\mathbf{r}-\mathbf{r}'\|^2} d\mathbf{r}' \tag{B.2}$$

where $\Omega$ is the compact support of the kernel $w_h$. Now, assuming that the perturbation can be expressed as

$$\delta p = Q(t) e^{\mathbf{i}\mathbf{k}\cdot\mathbf{r}} \tag{B.3}$$

Then,

$$\frac{d}{dt}Q(t) = 2\gamma\alpha I(h,k) Q(t) \tag{B.4}$$

where we have used the definition $I := I(h,k)$ which depends on the choice of the SPH kernel used.

$$I(h,k) = \int_\Omega \left(1 - e^{-\mathbf{i}\mathbf{k}\cdot(\mathbf{r}-\mathbf{r}')}\right) \frac{(\mathbf{r}-\mathbf{r}')\cdot\boldsymbol{\nabla} w_h}{\|\mathbf{r}-\mathbf{r}'\|^2} \tag{B.5}$$

When the leapfrog method is applied to the absolute stability model (B.4) we have

$$Q_{n+1} = Q_{n-1} + 2\Delta t \lambda Q_n, \quad \lambda = 2\gamma\alpha I(h,k) \tag{B.6}$$

The corresponding characteristic polynomial is given by $M_w(r) := r^2 - 2wr - 1$ with $w := \lambda\Delta t$. Since $w$ is real and positive, the leapfrog method has two distinct roots $r_\pm = w \pm \sqrt{1+w^2}$. Using the binomial expansion we have $r_+ = 1 + w + w^2/2 - w^3/8 + \ldots$, $|w| < 1$; i.e. for small $|w|$, one step of the mode $r_+$ of the leapfrog method agrees with the terms of order $\leq w^2$ in the exact solution and the remainder is bounded by a multiple of $w^3$. We formally have the time constraint as

$$\Delta t \leq \frac{1}{2}\frac{1}{\gamma\alpha I(h,k)} \tag{B.7}$$

For a Gaussian filter[19] we have $I(h,k) = 2/h^2$. In this case the stability condition becomes,

$$\Delta t \leq C_\alpha \frac{h^2}{4\gamma\alpha}, \qquad 0 < C_\alpha < 1 \tag{B.8}$$

where the parameter $C_\alpha$ depends on the dimensionality of the problem.

## References


[1] J. Monaghan, Simulating free surface flows with SPH, Journal of Computational Physics 110 (1994) 399 – 406. doi:https://doi.org/10.1006/jcph.1994.1034.

[2] M. Müller, D. Charypar, M. Gross, Particle-based fluid simulation for interactive applications, volume 2003, 2003, pp. 154–159.

[3] J. Monaghan, Smoothed particle hydrodynamics and its diverse applications, Annual Review of Fluid Mechanics 44 (2012) 323–346. URL: https://doi.org/10.1146/annurev-fluid-120710-101220. doi:10.1146/annurev-fluid-120710-101220.

[4] A. Colagrossi, M. Landrini, Numerical simulation of interfacial flows by smoothed particle hydrodynamics, Journal of Computational Physics 191 (2003) 448 – 475. doi:https://doi.org/10.1016/S0021-9991(03)00324-3.

[5] M. Antuono, A. Colagrossi, S. Marrone, D. Molteni, Free-surface flows solved by means of SPH schemes with numerical diffusive terms, Computer Physics Communications 181 (2010) 532 – 549. doi:https://doi.org/10.1016/j.cpc.2009.11.002.

[6] J. R. Clausen, Entropically damped form of artificial compressibility for explicit simulation of incompressible flow, Phys. Rev. E 87 (2013) 013309. doi:10.1103/PhysRevE.87.013309.

[7] P. Ramachandran, K. Puri, Entropically damped artificial compressibility for SPH, Computers & Fluids 179 (2019) 579 – 594. doi:https://doi.org/10.1016/j.compfluid.2018.11.023.

[8] A. Toutant, Numerical simulations of unsteady viscous incompressible flows using general pressure equation, J. Comput. Phys. 374 (2018) 822–842.

[9] A. Kajzer, J. Pozorski, A weakly compressible, diffuse-interface model for two-phase flows, Flow, Turbulence and Combustion 105 (2020). doi:10.1007/s10494-020-00164-8.

[10] D. Dupuy, A. Toutant, F. Bataille, Analysis of artificial pressure equations in numerical simulations of a turbulent channel flow, Journal of Computational Physics 411 (2020) 109407. doi:https://doi.org/10.1016/j.jcp.2020.109407.

[11] Z. Chen, Z. Zong, M. B. Liu, H. T. Li, A comparative study of truly incompressible and weakly compressible SPH methods for free surface incompressible flows, International Journal for Numerical Methods in Fluids 73 (2013) 813–829. URL: https://onlinelibrary.wiley.com/doi/abs/10.1002/fld.3824. doi:https://doi.org/10.1002/fld.3824.

[12] T. A. Zang, R. B. Dahlburg, J. P. Dahlburg, Direct and large-eddy simulations of three-dimensional compressible Navier–Stokes turbulence, Physics of Fluids A: Fluid Dynamics 4 (1992) 127–140. doi:10.1063/1.858491.

[13] F. D. Stacey, B. J. Brennan, R. D. Irvine, Finite strain theories and comparisons with seismological data, Geophysical Surveys 4 (1981) 189–232. doi:10.1007/BF01449185.

[14] N.-H. Mao, Empirical equation of state for high compression, Journal of Geophysical Research (1896-1977) 75 (1970) 7508–7512. doi:10.1029/JB075i035p07508.

[15] C. A. TRUESDELL, Finite deformation of an elastic solid. Francis d. Murnaghan. new york: Wiley; london: Chapman & hall, 1951. 140 pp. $4.00, Science 115 (1952) 634–634. doi:10.1126/science.115.2997.634-a.

[16] L. Knopoff, J. N. Shapiro, Pseudo-grüneisen parameter for liquids, Phys. Rev. B 1 (1970) 3893–3895. URL: https://link.aps.org/doi/10.1103/PhysRevB.1.3893. doi:10.1103/PhysRevB.1.3893.

[17] J. P. Morris, P. J. Fox, Y. Zhu, Modeling low reynolds number incompressible flows using SPH, Journal of Computational Physics 136 (1997) 214 – 226. doi:https://doi.org/10.1006/jcph.1997.5776.

[18] P. W. Cleary, J. J. Monaghan, Conduction modelling using smoothed particle hydrodynamics, Journal of Computational Physics 148 (1999) 227 – 264. doi:https://doi.org/10.1006/jcph.1998.6118.

[19] D. J. Price, Smoothed particle hydrodynamics and magnetohydrodynamics, Journal of Computational Physics 231 (2012) 759–794. URL: http://dx.doi.org/10.1016/j.jcp.2010.12.011. doi:10.1016/j.jcp.2010.12.011.

[20] S. Adami, X. Hu, N. Adams, A generalized wall boundary condition for smoothed particle hydrodynamics, Journal of Computational Physics 231 (2012) 7057 – 7075. doi:https://doi.org/10.1016/j.jcp.2012.05.005.

[21] L. Hu, Q. HongFu, C. FuZhen, S. Chao, A particle refinement scheme with hybrid particle interacting technique for multi-resolution SPH,

762 Engineering Analysis with Boundary Elements 118 (2020) 108 – 123.
763 doi:https://doi.org/10.1016/j.enganabound.2020.06.001.

764 [22] J. Monaghan, J. Kajtar, SPH particle boundary forces for arbitrary
765 boundaries, Computer Physics Communications 180 (2009) 1811 – 1820.
766 doi:https://doi.org/10.1016/j.cpc.2009.05.008.

767 [23] S. Marrone, A. Colagrossi, A. Di Mascio, D. Le Touzé, Prediction of
768 energy losses in water impacts using incompressible and weakly com-
769 pressible models, Journal of Fluids and Structures 54 (2015) 802 – 822.
770 doi:https://doi.org/10.1016/j.jfluidstructs.2015.01.014.

771 [24] S. Marrone, M. Antuono, A. Colagrossi, G. Colicchio, D. Le Touzé,
772 G. Graziani, $\delta$-sph model for simulating violent impact flows, Com-
773 puter Methods in Applied Mechanics and Engineering 200 (2011)
774 1526–1542. URL: https://www.sciencedirect.com/science/article/pii/
775 S0045782510003725. doi:https://doi.org/10.1016/j.cma.2010.12.
776 016.

777 [25] B. Buchner, Green water on ship-type offshore structures, Ph.D. Thesis,
778 Delft University of Technology (2002).

779 [26] S. Adami, X. Hu, N. Adams, A transport-velocity formulation for
780 smoothed particle hydrodynamics, Journal of Computational Physics
781 241 (2013) 292 – 307. doi:https://doi.org/10.1016/j.jcp.2013.01.
782 043.

783 [27] U. Ghia, K. Ghia, C. Shin, High-re solutions for incompressible flow
784 using the Navier-Stokes equations and a multigrid method, Journal of

Computational Physics 48 (1982) 387 – 411. doi:https://doi.org/10.1016/0021-9991(82)90058-4.

[28] A. M. Hofmeister, Pressure derivatives of the bulk modulus, Journal of Geophysical Research: Solid Earth 96 (1991) 21893–21907. doi:10.1029/91JB02157.

[29] C. Zhang, G. Xiang, B. Wang, X. Hu, N. Adams, A weakly compressible SPH method with WENO reconstruction, Journal of Computational Physics 392 (2019) 1 – 18. doi:https://doi.org/10.1016/j.jcp.2019.04.038.

[30] P. Ramachandran, PySPH: a reproducible and high-performance framework for smoothed particle hydrodynamics, 2016, pp. 122–129. doi:10.25080/Majora-629e541a-011.